Light Metals 2015
Edited by: Margaret Hyland
TMS (The Minerals, Metals & Materials Society), 2015

MATHEMATICAL MODELLING OF HALL-HÉROULT POT INSTABILITY AND VERIFICATION BY MEASUREMENTS OF ANODE CURRENT DISTRIBUTION

Valdis Bojarevics[1] and James W. Evans[2]
[1]University of Greenwich, Park Row, London SE10 9LS, UK
[2]Professor Emeritus, Dept. Matls. Sci. & Eng., University of California, Berkeley and Wireless Industrial Technologies, Inc.

Abstract

A software application based on the full MHD model of the aluminium electrolytic production cell is used to predict the liquid metal surface instability in a commercial Trimet operated potline. The results are compared with the electric current distribution variation in time over the anodes obtained from the measurement of magnetic fields by wireless sensors. The model incorporating full 3d busbar configuration predicts a critical instability excitation frequency 0.0259 Hz, which compares to the measured frequency of 0.0254 Hz. The mathematical software permits to analyse the sensitivity to the pot individual features like ACD, anode loads, ledge shape, bottom wear and busbar irregularities. The ability to monitor continuously the electric current distribution to high accuracy helps to control disturbances and to visualise the cell interior with the help of this numerical tool.

1. Introduction

Industrial aluminium production cells are highly optimised for magnetic field and electric current distribution in order to avoid MHD instabilities, increase the current efficiency and to maintain a stable electrolytic process during normal operation. The ability to monitor continuously the magnetic and electric field distributions to high accuracy is a key to control disturbances and deviations from a normal production process. Recent application of wireless sensors for the measurement of magnetic fields in commercial cells shows a possibility of a new flexible tool for the cell operation control [1]. The magnetic field measurements are available from the wireless sensors installed in pairs at each anode rod. Such a system was installed at TRIMET Aluminium, Hamburg, in early 2013 and has been reporting the magnetic field at each anode, the cell voltage and other parameters to the "cloud", every second for most of the time since then. A mathematical model enables the fields to be converted into individual anode currents, but for many purposes (including the present paper) the magnetic fields suffice as a surrogate for those currents. From a strict mathematical point of view, recovery of the electric currents in all the anodes requires a solution of non-uniquely defined inverse problem: to recover the source field from the resulting magnetic field in the surrounding space [2]. Of particular interest in this paper are MHD instabilities that lead to voltage fluctuations or, in extreme cases, short circuits between metal and anodes. Lossman [3] appears to have been the first to measure such instabilities, examining fluctuations in anode current, cell voltage and magnetic field (the last measured outside the cell near one corner). Segatz and Droste [4] used these results to validate a mathematical model intended to study MHD instabilities. That work was continued by Droste et al. [5]. Principal results from the modelling were the growth rates and oscillation periods of the MHD instabilities; both were calculated to decline with increasing anode-cathode distance (ACD). This result fully conforms to the known analytical criteria for the cell stability [6] and linear models accounting for realistic magnetic fields [7]. The fluctuation frequency shift with the magnetic field was observed experimentally and confirmed by the linear theory [8].

In the present paper a non-linear dynamically coupled mathematical theory and the software based on the full MHD model of the electrolysis cell is applied to a particular commercial cell [2,9]. Briefly, the full model computes time-dependent currents, voltages, magnetic fields, bath-metal interface shape and turbulent magnetically driven flow in the bath and liquid metal. Figure 1 is a schematic of the TRIMET potline showing a zoomed view to all the conductors that are part of the simulation, the conductors are colored by their computed currents. The temperatures of the bus bars are adjusted according to the computed Joule heating and losses to the air. The electric current in the individual anodes is computed at all times following the wave development on the interface between liquid layers. The dome shaped time average deformation of the metal surface is projected to the bottom of the whole anode block to account for the anode bottom burn-out effect for a constant ACD, except in the case of disturbance, such as an anode change operation. The electric current distribution in the liquid zone is computed from all the bus bar network connected to the anodes and cathode collectors, coupled with the cell interior details like the ledge profile, bottom shape, collector connections, electrolyte channels and the electrochemical voltage drop. The magnetic field is optionally recomputed at all times in order to follow the full magnetohydrodynamic wave and flow development. The detailed representation of the cell steel elements adds non-linearity to the overall magnetic field properties. The MHD response of different commercial cells is quite variable depending on their design (side-to-side, end-to-end, Soderberg, etc.), the line amperage, operational practices (tapping, anode change, bottom erosion, alumina feeding), and many other factors. The present investigation focuses on a particular cell type at the Trimet plant where the measurement data are available from the long term cell observation using the wireless sensor installation [1].

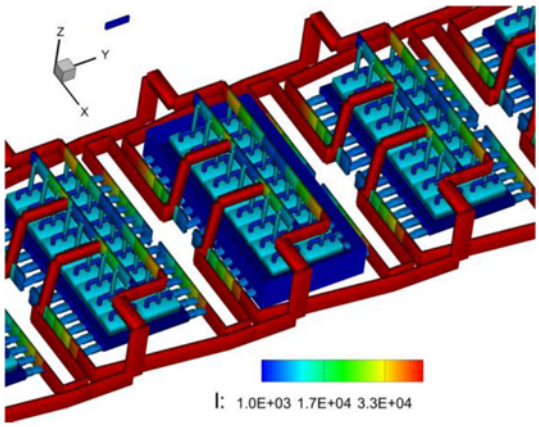

Figure 1. Busbar configuration for 180 kA Trimet cell.

2. Results of measurements compared to the modelling

Let us consider some specific cases of the measured distribution variation in time. Figure 2 gives the measured voltage and fields due to anode currents over a period of about 45 minutes on April 28th, 2014. The fields near each anode are surrogates for the current in each anode and are negative because, in the convention used in the measurements, the fields are negative behind the anode rods on the downstream side of the pot (see Figure 11 for the magnetic field computed at the level of sensors). Note that early in this period the pot is stable with a low voltage (low ACD) of ~4.2V and declining. At approximately 6:44 the fields and voltage start to oscillate and continue to do so until 7:15 when an increase in voltage to above 4.3V (presumably due to an increase in ACD) damps the oscillations. Stabilizing cell oscillations by increasing the ACD is well known in the industry and appears consistent with the calculations of Droste et al. [5] and the linear stability theory [6-9]. The oscillation period of the first half of the data of Fig. 2 was 38.5 seconds and for the second half 39.5 s, contrary to the expectation of a drop in period with increasing ACD suggested by those authors.

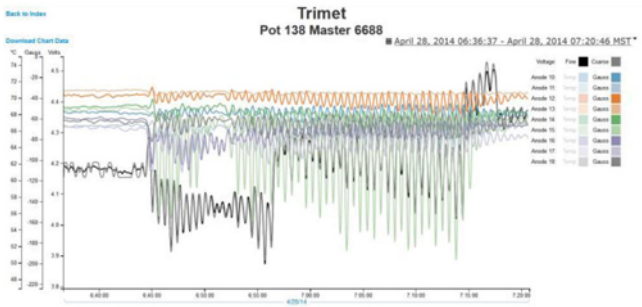

Figure 2. The measured voltage and fields due to anode currents over a period of about 45 minutes on April 28th, 2014.

The present full MHD simulation results are presented in the Figure 3 for a normally operated Trimet cell after a sloshing wave perturbation (known as 1,0 gravity wave mode) of a substantial 5 mm amplitude was imposed. Figure 3 shows the variation of the cell voltage and anode currents computed using the mathematical model for a normal case with the ACD of 4.5 cm, giving a calculated cell voltage of ~ 4.54V (dependent on given particular electrochemical voltage, pin and collector contact resistances); the metal depth was 17 cm. The calculations were started by imposing the perturbation on the bath-metal interface. There is a subsequent slow decay of this disturbance. The FFT of the current or voltage waves gives a peak at 0.0259 Hz which is an oscillation period of 38.46 seconds, consistent with the measured values (38.5 s) of the previous paragraph. Note that the voltage oscillation and the anode current oscillation have the same frequency which contrasts with earlier work where the voltage fluctuations had twice the frequency of the current fluctuations [4,5].

The results summarizing the cell parameter variation and the computed oscillation periods are shown in Table 1. An increase of the anode current oscillation period from 38.5 s to 40.65 s is detected when the ACD is reduced by 5 mm, leading to unstable wave development and the liquid metal short circuiting after about 7 minutes of applying the 5 mm perturbation. For unstable cases we observe typically a small deviation in the cell overall voltage drop oscillation period relative to the individual anode currents. The reduced ACD = 4 cm case gives 42.19 s period for the voltage, which is slightly larger than the anode current fluctuation period 40.65 s. The explanation of this may be related to the transitional nature of the oscillation as seen in Figure 4.

A similar increase of the oscillation period is found when reducing the metal level by 2 cm to 0.015 m corresponding, for instance, to the metal tapping operation, see Table 1 listing the main results of this study. The metal level decrease combined with the 5 mm amplitude sloshing perturbation leads to instability and the short circuiting of metal to anode in about 6 minutes. The cell can be stabilized either by raising the ACD, say by 5 mm from the normal 4.5 cm to 5 cm, or alternatively increasing the metal level by 3 cm to H_{al} = 0.020 m, see Table 1 and Figure 5. Segatz and Droste [4] reported improved stability (lower instability growth rates at higher metal depths) so Figure 5 is consistent with their result.

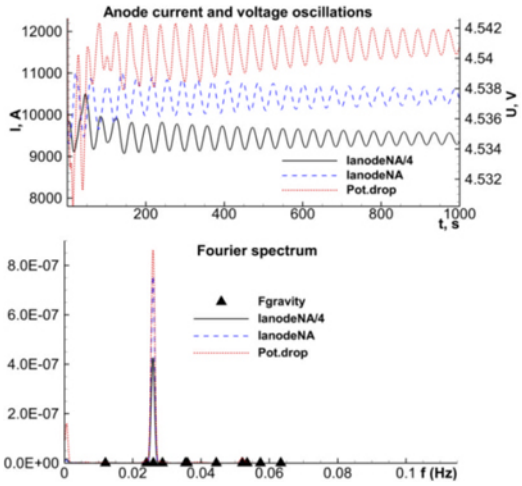

Figure 3. The normal 180 kA cell after 5mm sloshing (1,0) perturbation, ACD=0.045m, H_{al}=0.17m, anode number NA=18.

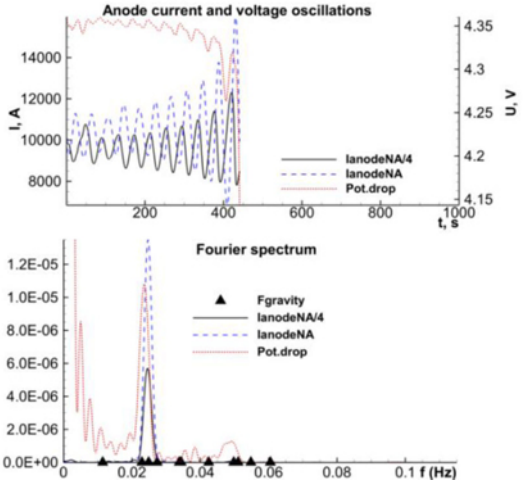

Figure 4. The reduced ACD=0.04m leads to instability and anode short circuiting for 180 kA cell after 5mm sloshing (1,0) perturbation (H_{al}=0.17m).

Several other cases were analysed using the mathematical model, summarized in Table 1. The initial sloshing wave perturbation corresponds to a relatively large period gravity wave (1,0) mode of the period T=83.54 s modified by the computed MHD interaction.

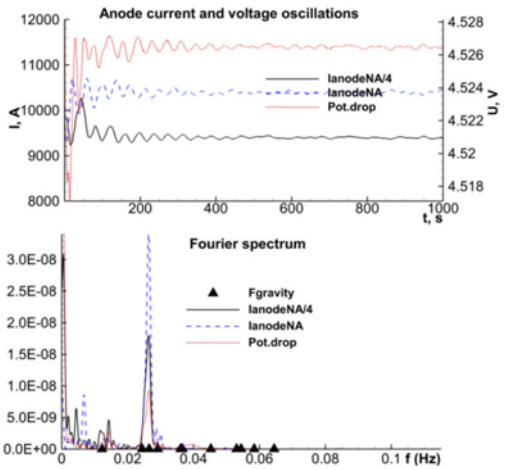

Figure 5. The increased metal level H_{al}=0.20m at normal ACD=0.045m makes the cell response very stable.

Table 1. Modelling results for the MHD wave response after the initial perturbation of longitudinal sloshing gravity wave mode (1,0) of 5 mm amplitude.

Case description	Period of the excited wave	Comments
Normal 180kA, ACD=0.045, H_{al}=0.17	38.46s	Initial 1,0 mode of T=83.54s modified by MHD action
Reduced ACD=0.04, normal H_{al}=0.17	40.65s (I_{an}) and 42.19s (U)	Unstable, short circuit at 440s
Increased ACD=0.05, H_{al}=0.17	37.04s	Fast damping
Normal ACD=0.045, H_{al}=0.15	39.37s (I_{an}) and 41.32s (U)	Unstable, short circuit at 350s
Normal ACD=0.045, H_{al}=0.20	37.88s	Fast damping
Normal ACD=0.045, H_{al}=0.17. No B(t)	36.63s	Fast damping
Normal cell, anode #1 change	38.46s (Ian) and 40.98s (U)	Unstable, short circuit at 500s
Normal cell, anode #1 change, ACD increase by 0.008m at 400 s	36.90 s (Ian) and 36.10s (U)	Unstable initially, stabilizes after 400s after ACD rise
Normal cell, anode #5 change	39.37s	Stable
Normal cell, anode N18 change	39.37s	Stable
Reduced ACD=0.04, H_{al}=0.17, I=160kA	40.65s	Stable
Normal ACD=0.045 H_{al}=0.17, 180kA, linear theory	41.67s	Oscillating MHD wave as in analytical theory

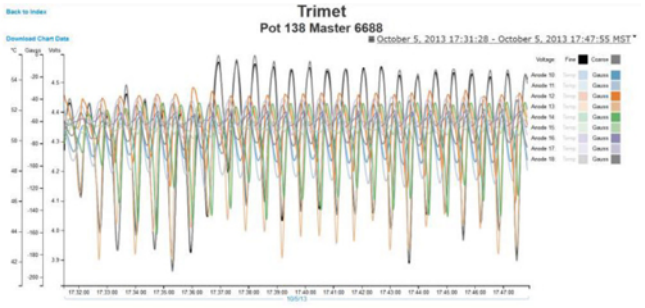

Figure 6. The measured period = 38.7s is close to the predicted normal cell response to a perturbation.

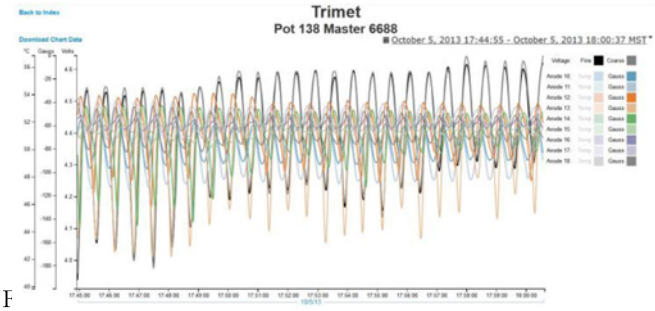

F
the predicted normal cell response.

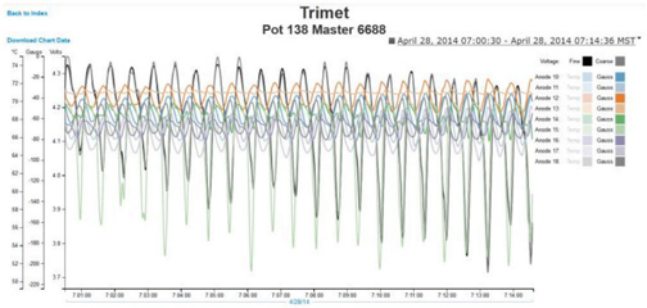

Figure 8. The case of the measured period = 39.4 s is close to the predicted cell response after reducing the metal level in tapping operation.

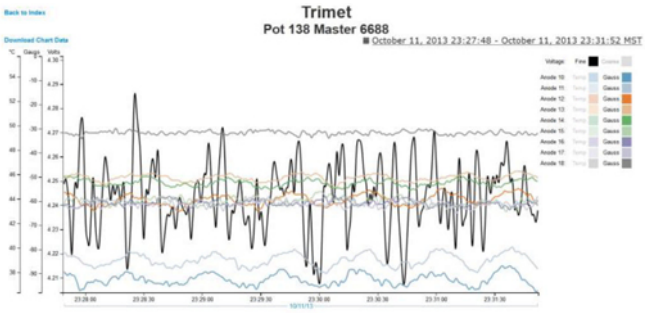

Figure 9. A measured case where voltage and magnetic field differences are not in sync exhibiting large time period oscillations close to the theoretical sloshing mode $T_{1,0}$ =83.5 s .

The period of the excited wave varies only slightly with the cell conditions, even though those conditions have a significant influence on the growth or decline of interface perturbations. The numerical predictions are in the same range as the measurements

for eight cases of MHD instability in the Trimet cell examined, and the period was found to lie between 35 seconds and 39.5 seconds. Several examples of the automatically recorded long term measurement extracts of the Trimet cell voltages and anode currents are shown in Figures 6-8. Those are typical responses to various day to day practices. A slightly unusual measurement type is shown in Figure 9.

3. Analysis of the anode change response

The numerical modeling tool permits to 'have a look inside' the cell during various disturbances or technological events. With the limitation of the available discussion space we choose to analyse in more detail the anode change process. The simulation for this uses the same setup as for the normal cell, except the chosen anode, or up to 4 anodes at the same time, are prescribed a 'frozen' bath condition at the bottom of the anode, effectively limiting the anode bottom electrical conductivity. Figure 10 demonstrates the electric current pick-up loss for anode #1 under the condition of the frozen bottom. The figure illustrates also the magnetic field component variation in the positions where the wireless sensors are located. The modeling results clearly indicate the very good correlation between the electric current and the magnetic field difference dBx = Bx2 - Bx1 (as measured by the sensors). Figure 11 gives an insight into the magnetic field distribution at the level of the sensors over the whole cell. The high gradient of the magnetic field variation is clearly indicating the position of individual anode rods.

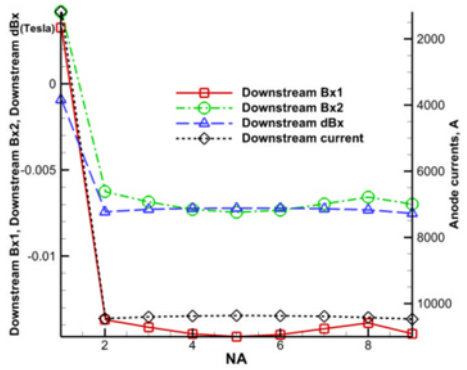

Figure 10. The magnetic field Bx components, the field difference in the sensor pairs and the electric current in the anodes computed for 180 kA cell at the sensor locations for the case of newly set anode #1.

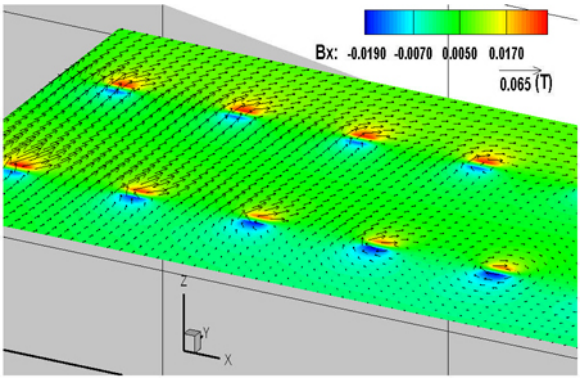

Figure 11. The magnetic field computed for 180 kA cell at the level of sensors at the top of anode rods.

From the series of simulation runs the anode #1 change is of particular interest because this leads to an instability of the MHD wave ending in the short circuit of the metal to anodes in about 8 minutes of the initial event (Figure 12). The run set up is the same as for the normal cell wave analysis shown in Figure 3, except for the effect of an anode change. The current in anode #1 (a corner anode at the side where the return row of cells is located) has been set to ~20% of its normal value to simulate the diminished current carried by a new anode for several tens of minutes after its placement in the cell. This unevenness in anode currents is seen to have a negative effect on cell stability, probably because of increased horizontal currents within the metal pool. A view at the metal interface topology in Figure 13 reveals a depression in the region of the changed anode and the growing sloshing wave at the other end of the cell. This is quite a contrast to the 'normal' cell metal surface in the stable cell shown in Figure 14.

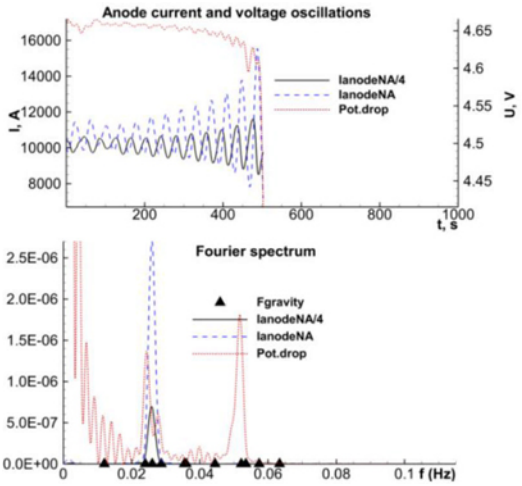

Figure 12. The normal cell response to the anode #1 (downstream left corner) change and (1,0) perturbation .

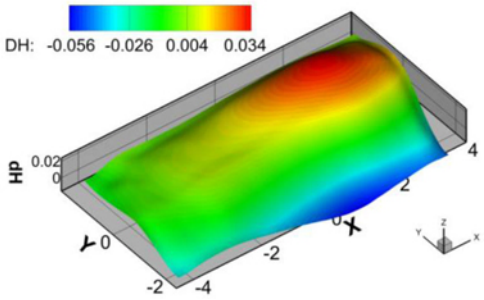

Figure 13. Metal interface just before the short circuiting after the anode #1 change (at the downstream lhs corner x=-4, y=2).

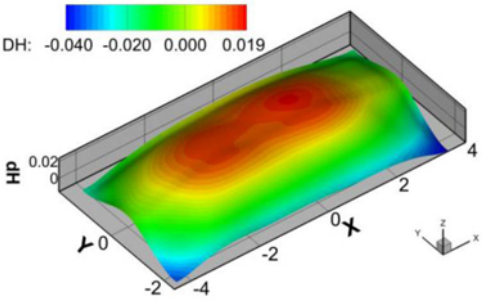

Figure 14. The normal cell metal interface after the longitudinal sloshing perturbation damping at t=1000 s.

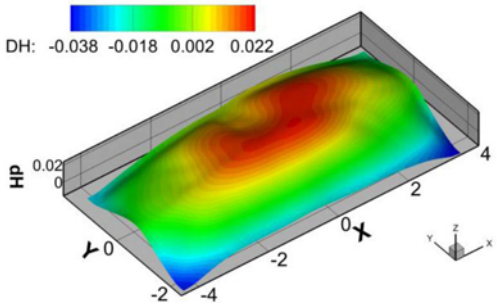

Figure 15. Interface after the anode #5 change, note the permanent stable depression below anode #5.

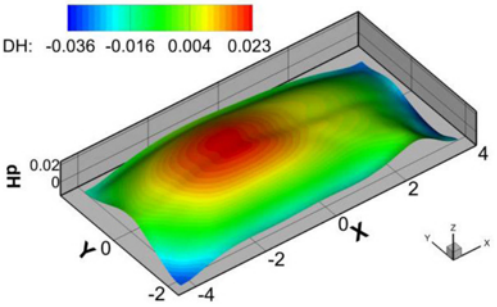

Figure 16. The stable interface shape after the corner anode #18 change (at the upstream rhs corner x=4, y=-2).

The effect of the interface depression under the changed anode is detected for other anode numbers. For instance, Figures 15 and 16 show the metal surface shape after the wave settles to a new stable interface shape for the anodes #5 and #18 being changed, respectively. The middle anode #5 gives a clear evidence of the depression, while the #18 corner is quite low next to the rather elevated interface in the neighbor position. The replacement of anode #5 or anode #18 (corner anode) did not appear to induce instability. The downward displacement of the interface below anode #5 in Figure 15 is remarkable and can be explained by the horizontal currents from the neighbor anodes connecting to the cathode collector beneath the poorly conducting anode. The direct action of the vertical electromagnetic force component F_z is not sufficient to explain this, because of the sign change for the radially incoming electrical current density beneath the disrupted anode.

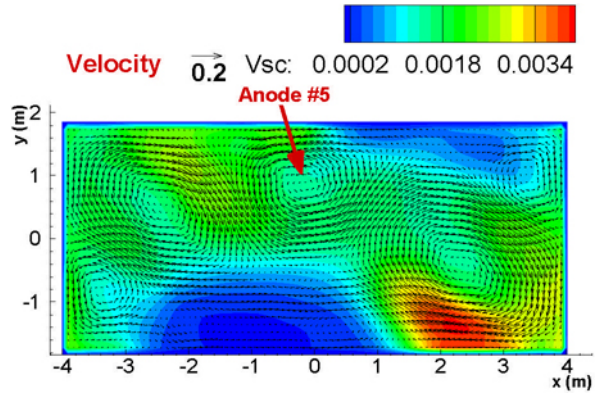

Figure 17. The velocity field in the liquid metal after the anode #5 change.

The mechanism leading to the appearance of depression is related to the metal velocity forming a vortex structure in the location of the anode #5, as seen in the Figure 17. Such local vortex is absent in the 'normal' cell velocity field shown in the Figure 18.

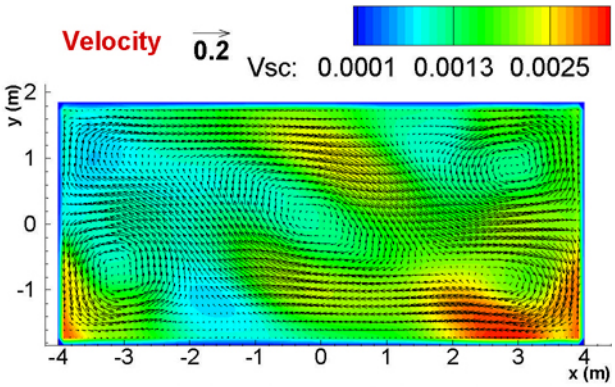

Figure 18. The velocity field and effective turbulent viscosity distribution in liquid metal after the long-term simulation 1000s.

The vortex in the liquid metal appears due to the local radially inward directed electric current in the aluminium layer as shown in Figure 19. The vortex rotation direction depends on the local vertical magnetic field Bz, but this results always in a depression of the interface due to the centrifugal force Fc ~ v_φ^2, as schematically explained in Figure 20.

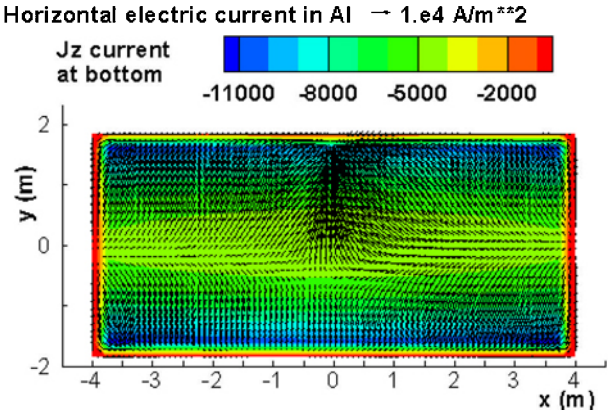

Figure 19. The electric current distribution in the liquid metal after the anode #5 change.

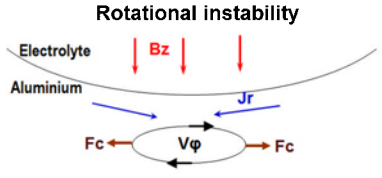

Figure 20. Schematic explanation to the origin of the dip in the liquid metal after the anode #5 change.

This theory seems to be supported by other anode #s changed, for instance the anode #18 case shows the new vortex in the corner beneath the anode #18, see Figure 21.

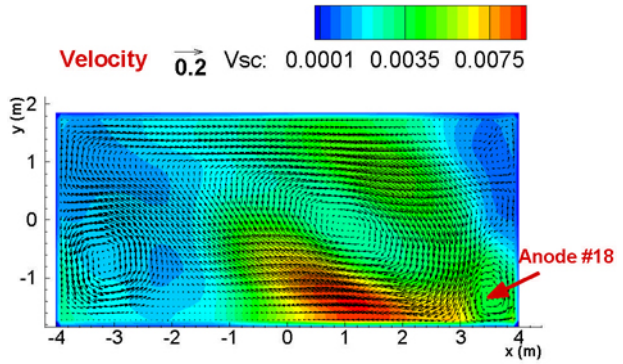

Figure 21. The velocity field in the liquid metal after the anode #18 change.

The predicted instability in the case of the anode #1 change is investigated further by imposing the condition that the whole anode block is raised at a time moment when the instability is starting. Figure 22 illustrates this result when the ACD was increased (from 0.045 m) by 8 mm at the time 400 s from the anode change start. This can be compared to Figure 12 where the instability led to short circuit at about 500 s. The raised ACD clearly stabilizes the magnetically excited wave.

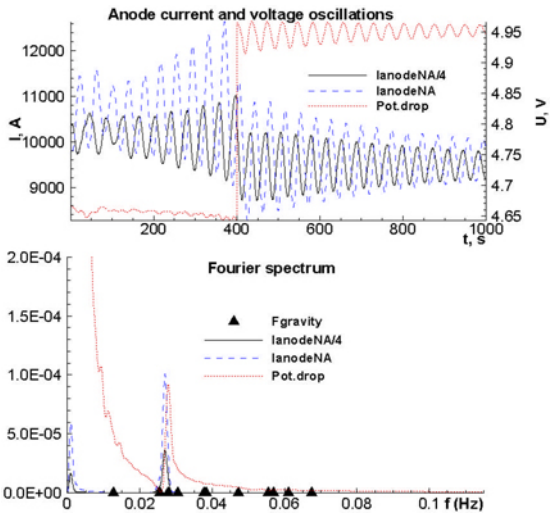

Figure 22. The normal cell response to the anode #1 (downstream left corner) change and (1,0) perturbation leading to instability, which is blocked rising the ACD by 8 mm at 400 s time moment.

Conclusions

The MHD model for the non-linear cell stability analysis is applied to the Trimet 180 kA cell to compare the measured results of the anode currents using wireless sensors. A close correlation is found between the numerical predictions and the measured results in most of the perturbation cases. The modelling offers insight to the cell dynamic events like the metal surface deformation under the anode change operation, wave stabilization at ACD rise or loss of stability in other situations. There are complicated cases requiring further studies based on the combination of the observation, measurements and numerical modelling, particularly for larger amperage cells where the nonlinear effects and the magnetic field non-uniformities are more expressed.

References

1. A. Lutzerath, J. W. Evans and R. Victor, On-line monitoring of anode currents; Experience at Trimet, Light Metals 2014 (Ed: J. Grandfield), The Minerals Metals and Materials Society, 2014, pp. 739-742.
2. V. Bojarevics, J. W. Evans. "An Application of the Inverse Solution for Electric Current Distribution from Magnetic Field Measurements in Aluminium Electrolysis Cells", Journal of Iron and Steel Research, International, 2012, 19, 1-1, pp. 561-565.
3. G. Lossman in Light Metals 1992, (Ed.: E.R. Cutshall), The Minerals Metals and Materials Society, 1992, pp. 441-447.
4. M. Segatz and C. Droste, in Light Metals 1994 (Ed.: U. Mannweiler), The Minerals, Metals and Materials Society, 1994, pp. 313-322.
5. C. Droste, M. Segatz and D.Vogelsang, in Light Metals 1998 (Ed.: B. Welch), The Minerals, Metals and Materials Society, 1998, pp. 419-428.
6. V. Bojarevics and M. V. Romerio. Long waves instability of liquid metal-electrolyte interface in aluminium electrolysis cells: a generalization of Sele's criterion. Eur. J. Mech., B/Fluids, 13 (1994), no 1, pp. 33-56.
7. N.Urata, in Light Metals 2005 (Ed.: H. Kvande), The Minerals, Metals and Materials Society, 2005, pp. 455-460.
8. R. Von Kaenel and J.P. Antille. Magnetohydrodynamic stability in alumina reduction cells. Travaux, 23 (1996), no. 27, pp. 285-297.
9. V. Bojarevics, K. Pericleous. Comparison of MHD Models for Aluminium Reduction Cells. In Proceedings of TMS Light Metals (2006), pp. 347-352.